Front. Optoelectron. China 2010, 3(1): 92–98
DOI 10.1007/s12200-009-0080-2

RESEARCH ARTICLE

Design of photosensitive microstructured polymer optical fibers

Hwa-Yaw TAM (✉)[1], Kei-Chun Davis CHENG[1], Guiyao ZHOU[1,2], Ming-Leung Vincent TSE[1]

1 Photonics Research Centre, Department of Electrical Engineering, The Hong Kong Polytechnic University, Hong Kong, China
2 Key Laboratory of Metastable Materials Science and Technology, Yanshan University, Qinhuangdao 066004, China

Abstract We propose a new hole-assisted polymer optical fiber design to eliminate the influence of dopant diffusion and to increase the ultra violet (UV) writing efficiency in fiber Bragg grating inscription. The optical waveguide is formed inside a solid core polymethyl methacrylate (PMMA) doped with photosensitive *trans*-4-stilbenemethanol, surrounded by a ring of three large air holes with double cladding. We determined a map of the single-mode and multi-mode phase transitions using a finite-element-based vectorial optical mode solver. A wide range of geometrical configurations for the single-transverse-mode (HE11) propagation in the visible was obtained. The design is optimized to operate at the low optical loss wavelengths of 580 and 770 nm.

Keywords microstructured polymer optical fibers (mPOFs), photosensitivity, fiber Bragg gratings, dopant diffusion

1 Introduction

Polymethyl methacrylate (PMMA) is the most commonly used material for microstructured polymer optical fibers (mPOFs). PMMA has much lower cost and larger strain extendibility over silica; it is often used in fiber sensing applications. Fiber Bragg grating (FBG) written in the PMMA mPOF was initially reported in 2005 [1]. However, it was reported that the presence of several rings of air holes in the mPOF cladding would increase scattering, resulting in significant reduction in the optical intensity of the ultra violet (UV) writing-beam. A long exposure of higher UV intensity laser source can be used to compensate for the loss of intensity due to the scattering, but it is adversely susceptible to physical damage within the fiber core [2]. Moreover, dopant diffusion from core to cladding affects the transmission properties inside the core. These effects should be considered when designing photosensitive mPOFs. In view of these problems, we carried out several research studies on the development of enhanced UV photosensitive polymers to improve the writing efficiency of FBGs in single-mode POFs in the past [3–6].

In this paper, we propose a new fiber design using the enhanced UV photosensitive PMMA polymer for efficient FBG writing. A double cladding fiber design with three air holes surrounding the core can maintain single-mode propagation with low confinement loss. This minimizes scattering of UV writing-beam and reduces the influence of dopant diffusion at the core region. Furthermore, it possesses single-mode guidance at visible wavelengths where low attenuation loss window of PMMA occurs.

In our work, a vectorial optical mode solver (Mode Solutions™ by Lumerical) based on a finite element method (FEM) was used to study the fiber design. We investigated the modal behavior by tailoring the dimensions of the structure, such that the single-mode propagation was found for maximum effective core size and bridge. Two operating wavelengths, 580 and 770 nm, were used in the simulation. The chosen wavelengths coincide with two of the minima of the PMMA attenuation profile, with values of ~0.07 and ~0.7 dB/m, respectively. Note that the attenuation of PMMA at 1550 nm is > 50 dB/m.

2 Design of a three-hole-assisted PMMA optical fiber with double cladding

The proposed design comprises double-clad layers, in which the inner cladding region is made of *trans*-4-stilbenemethanol (TS)-doped PMMA and the outer cladding is made of undoped PMMA, as shown in Fig. 1. We found that fiber Bragg grating can be written in TS-doped

Received August 1, 2009; accepted August 19, 2009

E-mail: eehytam@polyu.edu.hk

PMMA with a 325 nm laser beam in ~10 minutes. Inside the TS-doped region, the fiber core for the single-mode propagation is formed by the three large surrounding air holes. The effective core is located far away from the inner/outer cladding region, thus the influence of dopant diffusion (as shown in Fig. 2) can be minimized. Figure 2 shows that in the generic PMMA polymer optical fibers (POF) preform with no air hole, a significant dopant diffusion effect takes place from the core to the cladding during the polymerization of the core material.

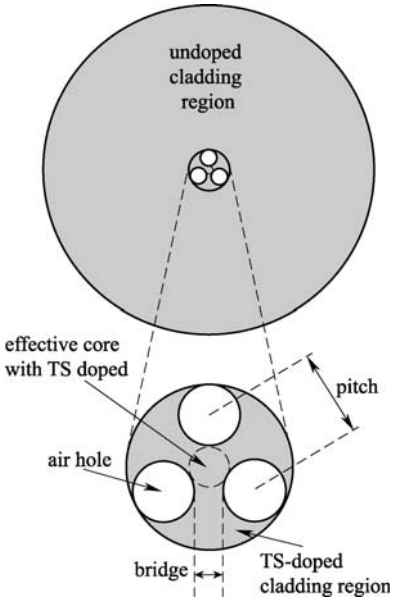

Fig. 1 Schematic diagram of PMMA hole-assisted fiber with a three-hole and double-clad structure

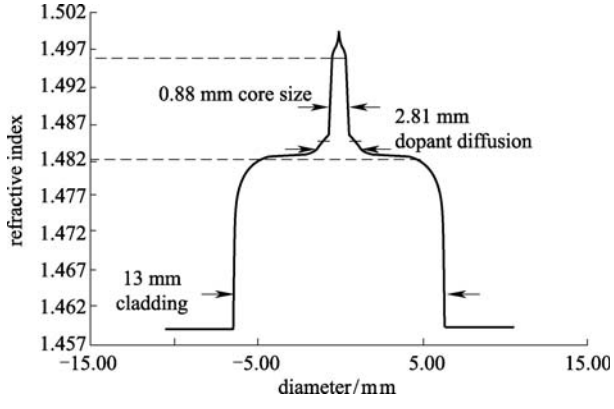

Fig. 2 Measured refractive index profile of a photosensitive POF preform determined by 2600 Plastic Optical Fiber Preform Analyzer, Photon Kinetics (Ltd)

3 Modal properties

The modal behavior of the three-hole-assisted PMMA optical fiber with double cladding was characterized by using the optical mode solver with circular perfectly-matched-layer (PML) boundary conditions [7]. The measured refractive index depicted in Fig. 3 was used for the simulation. The index measurement was fitted with a single exponential-decay relation of the form:

$$n(\lambda) = A\exp\left(\frac{-\lambda}{t}\right) + B, \tag{1}$$

where n is the refractive index of PMMA, A is the initial value of refractive index, t is a decay constant, B is the minimum value of the refractive index, and λ is the wavelength of light. A best-fitting curve was obtained with the calculated parameters ($A = 1.670 \pm 0.153$, $B = 1.493 \pm 0.001$, $t = 90.476 \pm 2.869$).

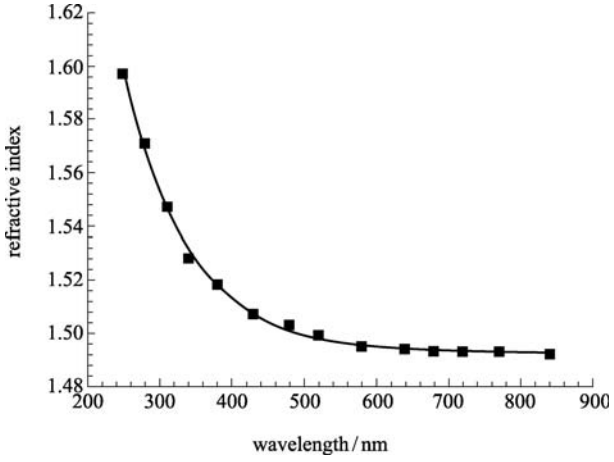

Fig. 3 Measured refractive index of bulk TS-doped PMMA sample as a function of wavelength (250–850 nm) which is determined by spectroscopic ellipsometry (solid line: fitting curve)

We studied the transverse magnetic fields of each mode propagating in the structure (diameter of effective core is 2.8 μm, bridge thickness is 1.35 μm, diameter of air hole is 8 μm, diameter of TS-doped and undoped cladding regions are 19 and 40 μm, respectively) at the operating wavelength of 580 nm. It was observed that multi-mode propagation with the first five modes (fundamental modes: HE11a- and HE11b-like, and the next higher order modes: TE01-, TM01- and HE21-like) were excited in the effective core. With group theoretical argument of n-fold rotation symmetry [8], HE11a- and HE11b-like modes are degenerate pairs with two-fold polarization, whereas TE01- and TM01-like modes are non-degenerate pairs. HE21a- and HE21b-like modes are not readily distinguished in the structure and only one HE21 mode can be found.

The field distribution of the first four propagation mode groups is shown in Fig. 4. The HE11-like mode in Fig. 4(a) that exhibited a Gaussian-like field distribution with triangular shape is well confined in the core surrounded

by the three air holes. This reveals that the confined mode excited far away from the inner/outer cladding boundary. Therefore, the mode would not be affected by the persistent doping diffusion from TS-doped cladding region to the outer undoped region.

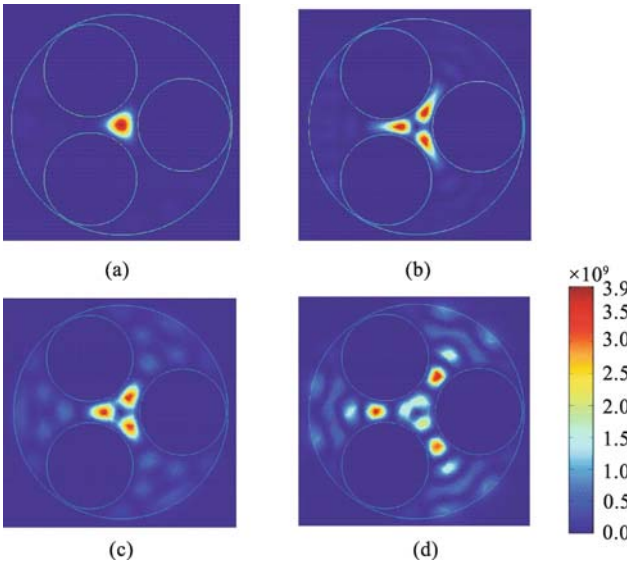

Fig. 4 Longitudinal component of time-averaged Poynting vector. (a) HE11-like mode of three-hole structure; (b) TE01-like mode of three-hole structure; (c) TM01-like mode of three-hole structure; (d) HE21-like mode of three-hole structure (color-coded scale is in arbitrary unit)

With known refractive indices of TS-doped PMMA, their effective indices and confinement loss of the five propagation modes can be determined (as shown in Table 1). The effective index of the HE11-like mode is well separated from the other modes and the index of the bulk TS-doped PMMA. The associated confinement loss is at least five orders of magnitude (in dB scale) lower than that of the higher-order modes. According to the multi-mode rejection ratio (MMRR) [9], this fiber geometry can be regarded as effectively single mode for long fiber-length application (i.e., several meters for a wavelength of 580 nm). In our case, a short fiber length is preferred so that the optimization of the design for strictly single-mode operation is required.

Table 1 Calculated mode effective indices of structure

mode	effective refractive index	confinement loss/(dB·m^{-1})
HE11a-like	1.48966	2.973×10^{-10}
HE11b-like	1.48965	1.479×10^{-10}
TE01-like	1.48456	2.925×10^{-5}
HE21-like	1.48433	3.352×10^{-4}
TM01-like	1.48398	1.132×10^{-5}

4 Map of single-mode phase transition

The cut-off wavelength for the three-hole-assisted PMMA optical fiber with different effective core diameter was investigated, and the result is illustrated in Fig. 5. In this simulation, the air hole sizes varied, and the bridge thickness was fixed at 1.1 μm. In Fig. 5, two curves of cut-off wavelengths represent the two phase transitions of the fundamental mode (HE11) and the next higher-order mode cutoffs take place, creating a region of single-mode propagation amid the two curves. For comparison, generic PMMA POF with no hole (shown as an overlap in Fig. 5) requires smaller core size to support single-mode propagation at the same wavelength. Such small core fiber is difficult to fabricate, and at the same time, further enhances the index variation due to an influence of doping diffusion at the doped/updoped boundary.

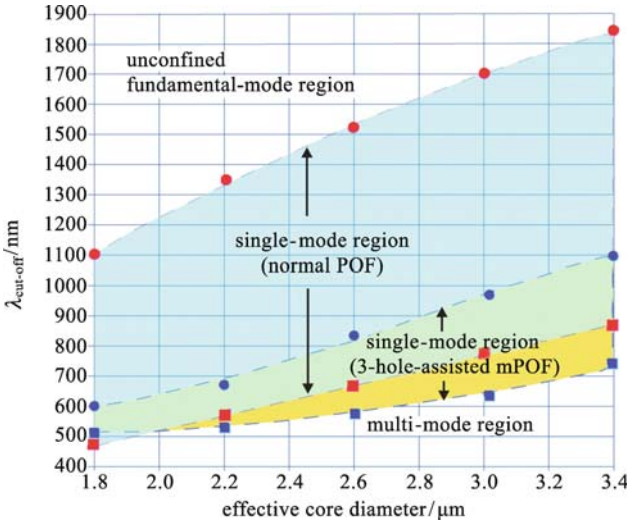

Fig. 5 Single-mode phase transition as a function of an effective core diameter for three-hole-assisted PMMA optical fiber and PMMA-based POF (bridge thickness is 1.1 μm)

The effect of the bridge thickness on the cut-off wavelength was also investigated, and the simulation results for the case of 2.6 and 3.4 μm effective core diameters are shown in Figs. 6(a) and 6(b), respectively. It was found that the upper limits of bridge thickness of two different core sizes were 1.46 and 1.83 μm, respectively. Beyond the limit, the bridge thickness became so large that some unidentified spurious modes were quasi-confined inside the bridge, leading to a deterioration of confinement loss. The fundamental mode transition was less sensitive to the bridge thickness. Nevertheless, a wide region of single-mode propagation was observed. These results along with those from Fig. 5 and Fig. 6(b) reveal that the tolerance of the core size and bridge thickness were sufficiently large (±16% and ±41%, respectively, at a wavelength of 770 nm) for the single-mode propagation.

It alleviated the difficulty caused during the preform fabrication and fiber drawing process.

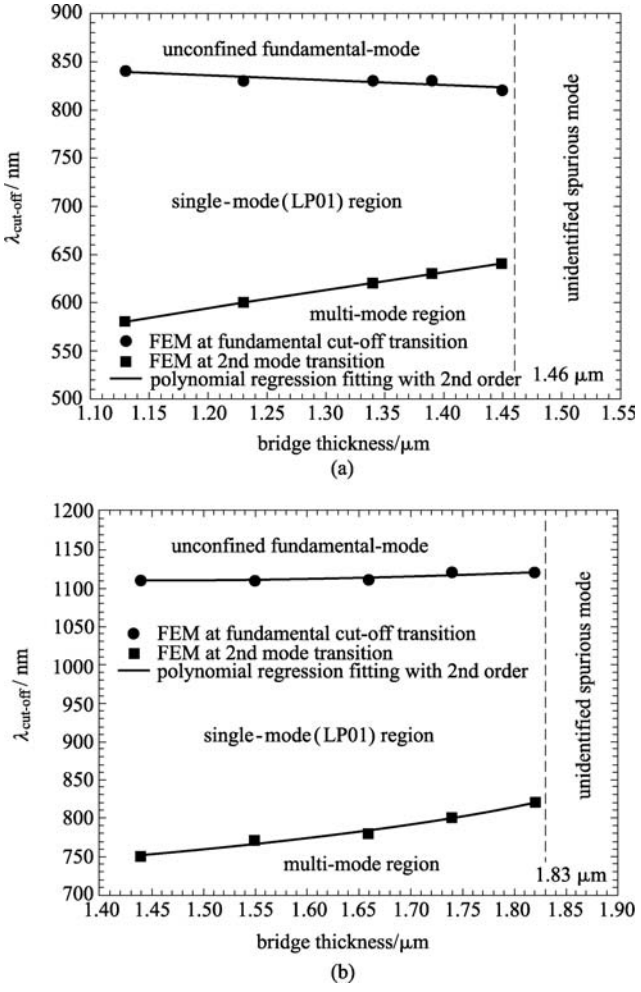

Fig. 6 Single-mode phase transition as a function of bridge thickness on three-hole-assisted PMMA optical fiber with an effective core diameter. (a) 2.6 μm; (b) 3.4 μm

5 Study of effective mode area

Setting the bridge thickness to 1.1 μm, the effective mode area of the three-hole-assisted PMMA optical fiber as a function of the effective core diameter within two phase transitions was investigated. The simulated effective mode area was calculated by [10]

$$A_{\text{eff}} = \frac{(\iint |E|^2 \mathrm{d}x\mathrm{d}y)^2}{\iint |E|^4 \mathrm{d}x\mathrm{d}y}, \tag{2}$$

where E is the amplitude of E-field intensity and can be determined by the mode solver.

The effective mode area moderately increased by broadening the bridge thickness to its upper limit are shown in Figs. 7(a) and 7(b).

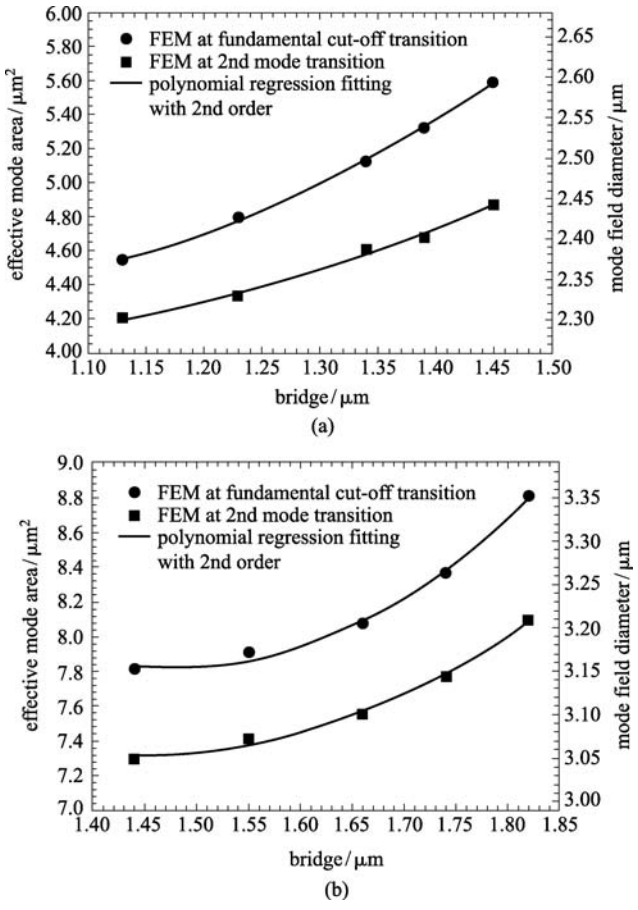

Fig. 7 Effective mode area and mode field diameter as a function of bridge thickness on three-hole-assisted PMMA optical fiber with an effective core diameter. (a) 2.6 μm; (b) 3.4 μm

We calculated the power coupling efficiency between the three-hole-assisted PMMA optical fiber and a commercial single-mode optical fiber (FiberCore SM600, with cut-off wavelength at 540 nm). The power coupling efficiency, T, was estimated by performing an overlap integral calculation using the formula [11]:

$$T = \frac{\left| \int \boldsymbol{E}_{\text{mPOF}} \cdot \boldsymbol{E}_{\text{SM600}} \mathrm{d}x\mathrm{d}y \right|}{\sqrt{\int |\boldsymbol{E}_{\text{mPOF}}|^2 \mathrm{d}x\mathrm{d}y \cdot \int |\boldsymbol{E}_{\text{SM600}}|^2 \mathrm{d}x\mathrm{d}y}}, \tag{3}$$

where $\boldsymbol{E}_{\text{mPOF}}$ and $\boldsymbol{E}_{\text{SM600}}$ are the electric fields of three-hole-assisted PMMA optical fiber and SM-600, respectively. The E-field intensity can be determined by the mode solver.

As the effective core diameter of the three-hole-assisted PMMA optical fiber approaches that of the SM600 (with effective mode area of 10.83 μm² and MFD of 3.7 μm), the coupling efficiency can be enhanced to 0.9, where the effective core diameter of the fiber is 3.4 μm (bridge thickness is 1.55 μm).

6 Optimized parameter of geometry

The effective core diameter and the bridge thickness for the three-hole-assisted PMMA optical fiber operating at 580 and 770 nm were optimized according to the results discussed so far. The optimized fiber parameters are presented in Table 2. The optical properties are presented in Table 3. and Fig. 8 It was revealed that the size of the TS-doped cladding region has negligible influence on the effective mode area. However, as the TS-doped cladding size increases, the confinement loss also increases. At doubling the size of the optimized dopant region, the confinement loss is less than $\sim 10^{-3}$ dB/m, which can be neglected for most sensing applications.

7 Study of optical power field distribution

In order to investigate the UV writing efficiency inside the effective core of the three-hole-assisted PMMA optical fiber for FBG inscription, we simulated the optical power field distribution inside the core region with optimized feature dimensions. With a two-dimensional (2D) simulation by Comsol FEMLAB, a plane wave of a wavelength of 325 nm (that is the UV writing wavelength) propagated transversally at normal incidence to the microstructure inside the TS-doped cladding region. The field distribution in two different orientations of the microstructure is presented in Figs. 9(a) and 9(b), with a wavelength of 325 nm, the electric field propagated from left to right (arrow denotes the field direction). The color-coded scale is in arbitrary unit. Figure 9(a) shows that the UV field lines penetrated through the bridge, resulting in a maximum optical power obtained the effective core. A uniform fringe pattern was observed inside the core region, leading to an enhancement in UV writing efficiency. It can be speculated that only a few large air holes inside the photosensitive region would not introduce significant scattering. Figure 9(b) shows that when the plane wave propagated normally through a large air hole, the optical power inside the effective core dropped significantly because of an existence of scattering and high contrast of refractive index between the solid core and air. Although the uniform fringe pattern can still be seen in the entire effective core, a reduction in optical power will cause inefficient FBG inscription.

We fabricated a three-hole-assisted PMMA optical fiber, and observed light guiding at 800 nm. A scanning electron microscope (SEM) image of the fiber is shown in Fig. 10. We aim to fabricate the proposed TS-doped fiber in the near future.

8 Conclusions

We have proposed a new design of three-hole-assisted PMMA optical fiber with double-cladding to eliminate the effect of dopant diffusion and to improve the UV writing efficiency. Its modal behavior excited inside the fiber was investigated so as to devise a relationship between the critical parameters such as cut-off wavelength, effective core diameter, and bridge thickness. Effective mode area and power coupling were studied for the optimized design. The optimized parameters and the associated optical properties of the design operating at 580 and 770 nm were obtained. The fabrication of the fiber with optimized geometry is being carried out and further experimental work such as optical bending loss, UV FBG writing performance with uniformity of doping and sensitivity of temperature/strain with this fiber design will be reported afterwards.

Table 2 Optimized dimensions of three-hole-assisted PMMA optical fiber at $\lambda = 580$ and 770 nm

wavelength/nm	optimized dimensions						
	outer diameter of cladding region/μm	diameter of dopant region/μm	diameter of air hole/μm	pitch/μm	bridge thickness (max)/μm	air filling fraction	effective core diameter (max)/μm
580	125.00	19.60	8.40	9.53	1.13	0.55	2.60
770	125.00	24.40	10.40	11.95	1.55	0.55	3.40

Table 3 Optical properties of three-hole-assisted PMMA optical fiber at $\lambda = 580$ and 770 nm

wavelength/nm	optical properties								
	operating wavelength/μm	refractive index of PMMA (doped)	refractive index of PMMA (undoped)	effective refractive index of LP01 mode	confinement loss/($dB \cdot m^{-1}$)	effective mode area of core (max)/μm^2	mode field diameter (MFD)/μm	power coupling to SM-600 standard fiber (fiber core)	insertion loss/dB
580	0.58	1.495	1.483	1.490	6.351×10^{-7}	4.206	2.314	0.724	1.403
770	0.77	1.493	1.482	1.487	2.715×10^{-7}	7.415	3.073	0.891	0.501

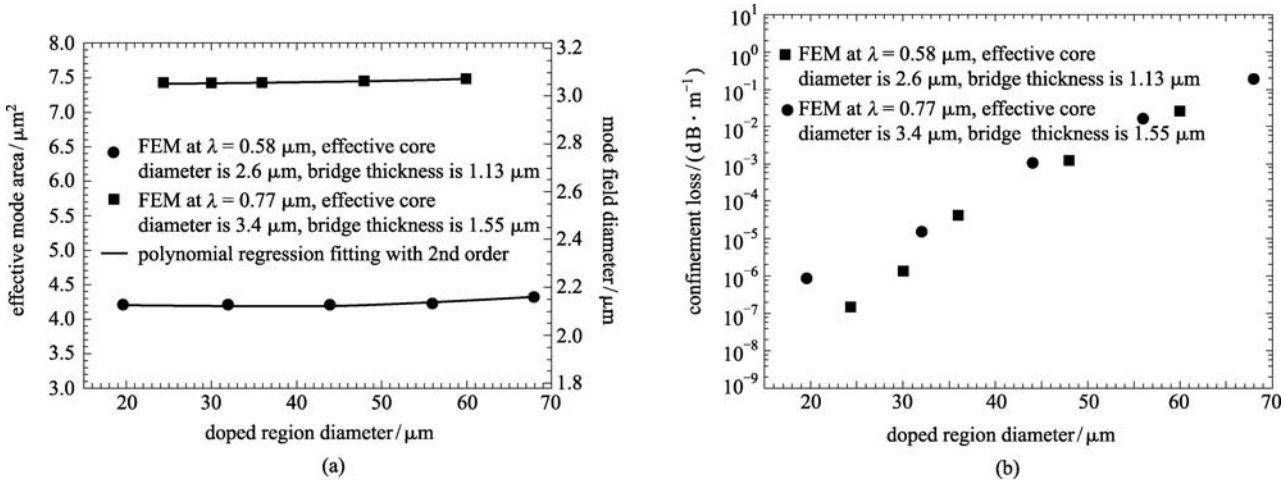

Fig. 8 Effective mode area and confinement loss as a function of doped region diameter on three-hole-assisted PMMA optical fiber with an effective core diameter of 2.6 μm and 3.4 μm, respectively. (a) Effective mode area; (b) confinement loss

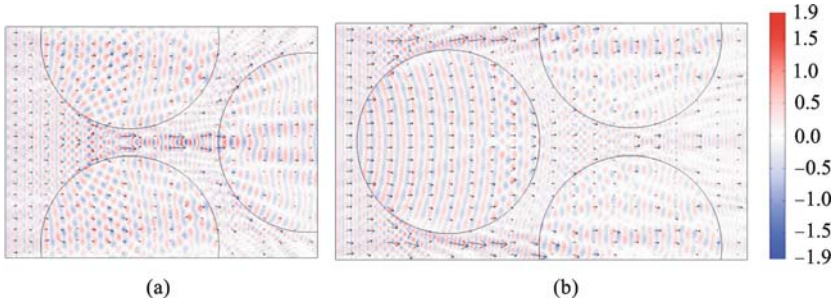

Fig. 9 Optical power distribution across three-hole-assisted PMMA optical fiber (core diameter is 3.4 μm, air holes are 10.4 μm, and bridge thickness is 1.55 μm) after propagation of a plane wave at normal incidence transversally to hole-assisted fiber. (a) Through bridge; (b) through air hole

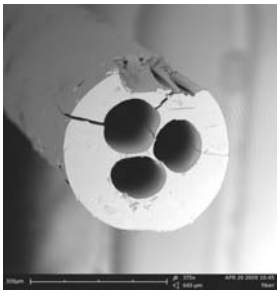

Fig. 10 SEM image of a three-hole-assisted PMMA optical fiber

Acknowledgements The authors acknowledge the funding support from the University Grants Council's Matching Grant of the Hong Kong Special Administrative Region Government under the Niche Areas Project J-BB9J and Central Research Grant of The Hong Kong Polytechnic University under Project G-U347.

References

1. Dobb H, Webb D J, Kalli K, Argyros A, Large M C J, van Eijkelenborg M A. Continuous wave ultraviolet light-induced fiber Bragg gratings in few- and single-mode microstructured polymer optical fibers. Optics Letters, 2005, 30(24): 3296–3298
2. Liu H Y, Liu H B, Peng G D, Chu P L. Observation of type I and type II gratings behavior in polymer optical fiber. Optics Communications, 2003, 220(4–6): 337–343
3. Yu J M, Tao X M, Tam H Y. *Trans*-4-stilbenemethanol-doped photosensitive polymer fibers and gratings. Optics Letters, 2004, 29 (2): 156–158
4. Yu J M, Tao X M, Tam H Y. Fabrication of UV sensitive single-mode polymeric optical fiber. Optical Materials, 2006, 28(3): 181–188
5. Tao X M, Yu J M, Tam H Y. Photosensitive polymer optical fibres and gratings. Transactions of the Institute of Measurement and Control, 2007, 29(3–4): 255–270
6. Tam H Y, Zhou G Y, Pun C F. US Patent, Application No. 12329545, 2008-07-01
7. Rogier H, De Zutter D. Berenger and leaky modes in optical fibers terminated with a perfectly matched layer. Journal of Lightwave Technology, 2002, 20(7): 1141–1148
8. Ren G B, Wang Z, Lou S Q, Jian S S. Mode classification and degeneracy in photonic crystal fibers. Optics Express, 2003, 11(11): 1310–1321
9. Uranus H P, Hoekstra H J W M, van Groesen E. Modes of an endlessly single-mode photonic crystal fiber: a finite element

investigation. In: Proceedings of Symposium IEEE/LEOS Benelux Chapter. 2004, 311–314

10. Iiyama K, Yamashita Z, Takamiya S. Design of dispersion flattened photonic crystal fiber with a large core and a concentric missing ring. In: Proceedings of 2005 IEEE/LEOS Workshop on Fibers and Optical Passive Components. 2005, 10–13
11. Wagner R E, Tomlinson W J. Coupling efficiency of optics in single-mode fiber components. Applied Optics, 1982, 21(15): 2671–2688